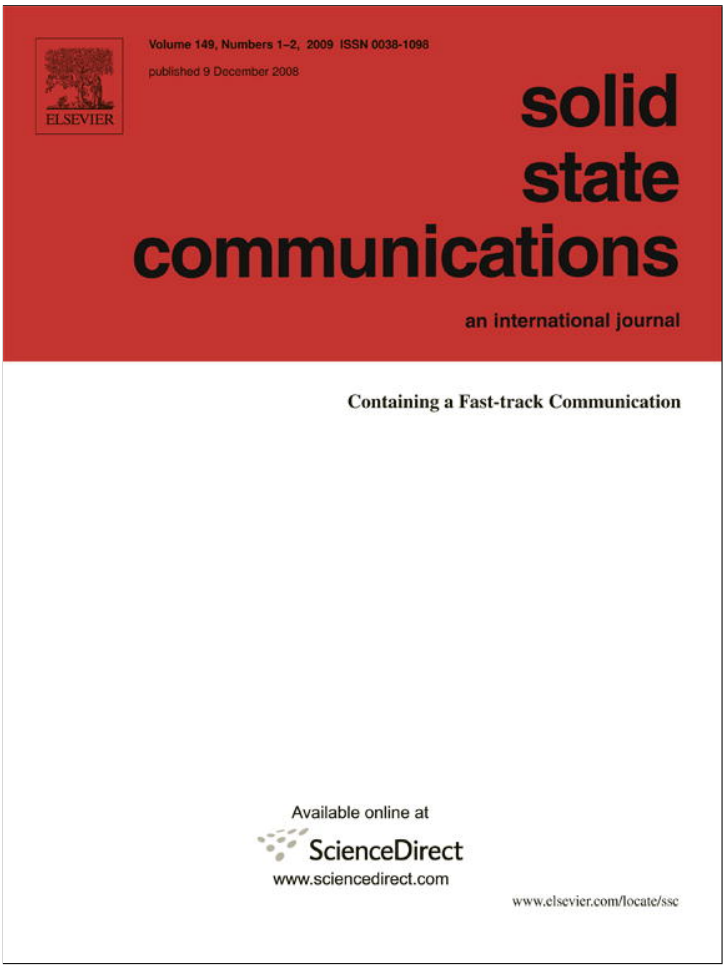

Solid State Communications 149 (2009) 10–13

Contents lists available at ScienceDirect

Solid State Communications

journal homepage: www.elsevier.com/locate/ssc

Effect of temperature on Raman scattering in hexagonal ZnMgO for optoelectronic applications

J.F. Kong [a], W.Z. Shen [a,*], Y.W. Zhang [b], X.M. Li [b], Q.X. Guo [c]

[a] Laboratory of Condensed Matter Spectroscopy and Optoelectronic Physics, Department of Physics, Shanghai Jiao Tong University, 1954 Hua Shan Road, Shanghai 200030, China

[b] State Key Laboratory of High Performance Ceramics and Superfine Microstructures, Shanghai Institute of Ceramics, Chinese Academy of Sciences, 1295 Ding Xi Road, Shanghai 200050, China

[c] Synchrotron Light Application Center, Department of Electrical and Electronic Engineering, Saga University, Saga 840-8502, Japan

ARTICLE INFO

Article history:
Received 16 September 2008
Accepted 20 October 2008 by R. Merlin
Available online 29 October 2008

PACS:
78.30.Fs
65.40.-b
63.20.-e
78.66.Hf

Keywords:
A. Thin films
C. Impurities in semiconductors
D. Phonons
D. Anharmonicity

ABSTRACT

We have carried out a detailed investigation of temperature-dependent micro-Raman scattering on hexagonal ZnMgO films with different Mg compositions (0–0.323). The phonon frequencies downshift and linewidths broadening of A_1 [longitudinal optical (LO)] and E_1(LO) modes can be well explained by a model involving the contributions of thermal expansion, lattice-mismatch-induced strain, and anharmonic phonon processes. We have elucidated the variation with Mg composition of the contribution of the three- and four-phonon processes in the anharmonic effect. The present work establishes an experimental base for the micro-Raman technique to monitor the local temperature during the ZnMgO-based device operation with a submicrometer spatial resolution.

1. Introduction

Wurtzite ZnO-based materials and related heterostructures have attracted a great deal of attention for blue lasers, ultraviolet (UV) light-emitting diodes, and UV photodetectors [1] due to their superior properties of direct wide bandgaps and large exciton binding energies which give rise to excitonic emission up to room temperature [2]. GaN-based materials are well known for the tendency of luminescence efficiency to drop dramatically with decreasing wavelength [3]. However, higher luminescence efficiency can still be achieved for higher Mg composition of ZnMgO alloys [4], which indicates that ZnMgO has great potential for use in UV region optoelectronic devices. Most of the research efforts to date have concentrated on the growth and study of ZnMgO epitaxial films, heterostructures, and quantum wells, which have been mainly prepared by molecular beam epitaxy [1,4], metal-organic epitaxial methods [5], and pulsed laser deposition (PLD) [6,7].

Efficient electron-hole recombination in ZnMgO/ZnO heterostructures has been recently realized, and the exploitation of their UV device application is the focus of current optoelectronics [4]. For high-power ZnMgO-based light emission applications, it is essential to monitor and eliminate the facet degradation, which is triggered by strong facet surface heating due to any possible nonradiative carrier recombination [8]. Raman scattering, as a fast, nondestructive, and contactless technique, is highly sensitive to the lattice temperature which allows us to use Raman spectroscopy as a temperature probe [9]. Temperature dependence of E_2 phonon modes has been employed to determine the local temperature of GaN diodes as a function of the operating voltage [10]. Moreover, since the size of the recording laser beam spot is determined by the laser wavelength and the numerical aperture of the objective lens, the availability of Raman microprobes opens the possibility of using Raman scattering as a local temperature assessment of power devices under operation with submicrometer spatial resolution.

In this paper, we have presented a comprehensive micro-Raman investigation of temperature- dependent Raman spectra of A_1 [longitudinal optical (LO)] and E_1(LO) modes in hexagonal ZnMgO films with different Mg compositions (0–0.323) in the temperature range from 83 to 578 K. In combination with detailed theoretical modellings for the frequencies downshift and linewidths broadening, we have clearly illustrated the temperature effect on the phonon frequency and linewidth, which establishes

* Corresponding author. Tel.: +86 21 54743242; fax: +86 21 54741040.
E-mail address: wzshen@sjtu.edu.cn (W.Z. Shen).

0038-1098/$ – see front matter © 2008 Elsevier Ltd. All rights reserved.
doi:10.1016/j.ssc.2008.10.024

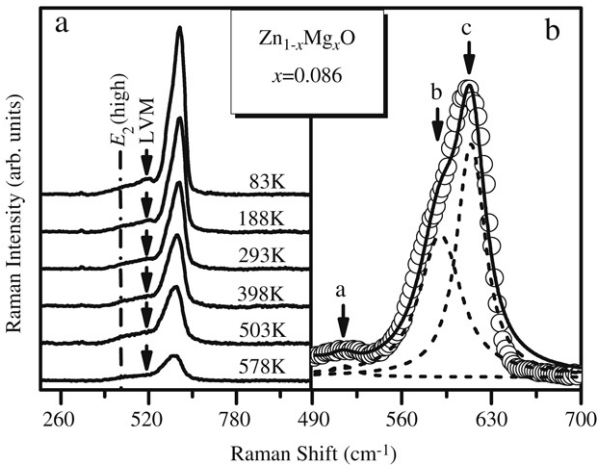

Fig. 1. (a) Temperature-dependent first-order micro-Raman spectra of $Zn_{0.914}Mg_{0.086}O$ and (b) Raman spectrum from $Zn_{0.914}Mg_{0.086}O$ at 83 K, where the solid curve fits results using three Lorentz peaks (dashed curves) with a: Mg-related LVM, b: A_1(LO), and c:E_1(LO).

an experimental base for monitoring the local temperature during the ZnMgO-based device operation.

2. Experiments

The studied $Zn_{1-x}Mg_xO$ thin films were deposited on (0001) α-Al_2O_3 substrates by PLD system employing a plasma oxygen or gaseous oxygen source at the temperature of 600 °C. During the deposition, the O plasma source was introduced by a plasma generator on the working voltage of 400 V and the current of 35 mA. Ceramic ZnMgO targets were ablated by a KrF excimer laser (Lambda Physik COMpex, wavelength of 248 nm, energy of 200 mJ/pulse, and repetition rate of 5 Hz). The crystallographic orientation was accessed by sharp and exclusive (0002) and (0004) x-ray diffraction peaks. The Mg composition was confirmed by x-ray photoelectron spectroscopy measurements (Quantum 2000). Temperature-dependent micro-Raman scattering spectra were recorded in a backscattering geometry of $z(x, -)\bar{z}$ configuration using a Jobin Yvon LabRAM HR 800UV system under the 325 nm line of a He–Cd laser. The employment of a 40 × optical microscopy objective with a numerical aperture of 0.5 will yield a laser spot size of ~0.8 μm.

3. Results and discussion

Fig. 1(a) presents the typical temperature-dependent first-order micro-Raman spectra of $Zn_{0.914}Mg_{0.086}O$. It is clear that the dominant peak can be attributed to the LO phonon mode, which shifts to high frequency and narrows with the decrease of temperature, accompanying the E_2 (high) mode [7] (dash-dotted curve) and the gradual appearance of an additional phonon mode centered at ~515 cm^{-1} (marked as arrows). In order to identify each part of the contribution, we have fitted the observed Raman spectra with Lorentz peaks. Fig. 1(b) shows the detailed analysis of the Raman spectrum for $Zn_{0.914}Mg_{0.086}O$ at 83 K (circles) with three peaks a, b, and c at about 515, 590, and 614 cm^{-1}, respectively. From the peak positions, we can assign peak a to the mixed mode of the ZnMgO, which originates from the Mg-related local vibrational mode (LVM) in ZnO [11], and peaks b and c to the A_1(LO)- and E_1(LO)-phonon modes of ZnMgO [12]. The above Lorentz fitting processes also help us obtain the detailed temperature and Mg-composition dependences of the phonon frequency and linewidth, and in the following we concentrate on the phonon characteristics of the A_1(LO) and E_1(LO) modes in the $Zn_{1-x}Mg_xO$ alloy.

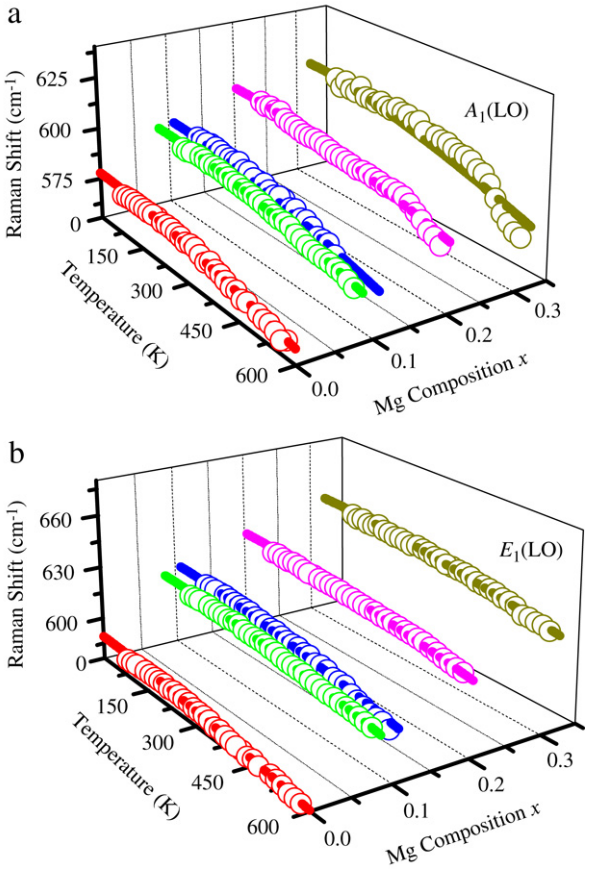

Fig. 2. Temperature-dependent Raman frequency of the (a) A_1(LO) and (b) E_1(LO) modes in ZnMgO with different Mg compositions. The solid curves are the theoretical calculation results with Eqs. (1) and (2).

Fig. 2(a) and 2(b) illustrate the frequencies of the A_1 (LO) and E_1(LO) modes with temperature. The downshift of the phonon frequency with the increase in temperature can be described by the perturbation model in which the frequency shift is mainly due to the effects of the thermal expansion, lattice-mismatch-induced strain, and the anharmonic coupling to other phonons [9, 10]. The Raman frequency can be expressed as a function of the temperature as:

$$\omega(T) = \omega_0(T) + \Delta\omega_e(T) + \Delta\omega_s(T) + \Delta\omega_d(T) \quad (1)$$

with ω_0 the harmonic frequency of the optical mode, $\Delta\omega_e(T)$ the contribution of thermal expansion or volume change, $\Delta\omega_s(T)$ the lattice and thermal mismatch between the ZnMgO thin films and sapphire substrate, and $\Delta\omega_d(T)$ the one due to the anharmonic coupling to phonons of other branches. The term $\Delta\omega_e(T)$ can be written as $\Delta\omega_e(T) = -\omega_0\gamma\int_0^T[\alpha_c(T') + 2\alpha_a(T')]dT'$, where γ is the mode Grüneisen parameter [13], α_c and α_a are the temperature-dependent linear thermal expansion coefficients parallel and perpendicular to the c axis, respectively [14]. The strain-induced term $\Delta\omega_s(T)$ can be given by $\Delta\omega_s(T) = [2a - (2c_{13}/C_{33})b]\varepsilon(T)$, with $\varepsilon(T)$ a temperature dependence of in-plane strain for the different thermal expansion coefficients between thin films and substrates [15]. The phonon deformation potentials a and b are supposed to be the same as those of E_2 (high) in ZnO [16] since those of A_1(LO) and E_1(LO) are not available. The elastic constants C_{13} and C_{33} of ZnO are taken from Ref. [17].

Taking into account cubic and quartic terms in the anharmonic Hamiltonian, we have the term $\Delta\omega_d(T)$ as [9,10,15]:

$$\Delta\omega_d(T) = M_1[1 + n(T, \omega_1) + n(T, \omega_2)] + M_2[1 + 3n(T, \omega_0/3) + 3n^2(T, \omega_0/3)] \quad (2)$$

Table 1
The best fitting parameters for Raman frequency [Eqs. (1) and (2)] and linewidth [Eq. (3)] of the A_1(LO) and E_1(LO) modes in hexagonal ZnMgO.

Raman modes	$Zn_{1-x}Mg_xO$ (x)	ω_0 (cm^{-1})	M_1 (cm^{-1})	M_2 (cm^{-1})	Γ_0 (cm^{-1})	N_1 (cm^{-1})	N_2 (cm^{-1})
A_1(LO)	0	579.6	−1.58	−0.35	11.2	3.52	0.81
	0.086	595.6	−1.69	−0.46	33.6	4.09	1.22
	0.108	596.8	−1.70	−0.51	36.0	4.26	1.32
	0.204	607.7	−1.75	−0.60	47.9	5.09	2.36
	0.323	613.2	−1.96	−0.80	51.6	5.89	3.15
E_1(LO)	0	589.4	−1.05	−0.17	12.7	1.71	0.29
	0.086	617.9	−1.40	−0.26	18.8	1.94	0.45
	0.108	621.1	−1.43	−0.28	19.9	2.04	0.49
	0.204	632.7	−1.49	−0.37	22.0	2.45	0.77
	0.323	645.1	−1.58	−0.47	28.6	2.57	0.91

where $n(T,\omega) = [\exp(\hbar\omega/k_BT) - 1]^{-1}$ is the Bose–Einstein function. In Eq. (2), the first term corresponds to the decay into two phonons of frequency ω_1 and ω_2 (three-phonon process), with $\omega_1 + \omega_2 = \omega_0$; while the second term accounts for the decay into three phonons (four-phonon process), considering simply equal frequency $\omega_0/3$. M_1 and M_2 are anharmonic constants which are related to the relative probability of the occurrence of each process. Generally, the simplest three-phonon process for optical phonon decay, proposed by Klements, is the decay into acoustic phonons of equal energy, $\omega_1 = \omega_2$, and opposite [15]. However, in the case of ZnMgO, the zone-center A_1(LO) and E_1(LO) cannot decay into two longitudinal acoustic (LA) or transverse acoustic (TA) phonons of equal frequency and the opposite wave vector in the three-phonon process due to the rather large energy gap between the acoustic and optical phonon branched ($2\omega_{LA,TA} < \omega_{LO}$). There is a possibility to decay into two phonons with different frequencies, which can be obtained from Ref. [13].

The solid curves in Fig. 2 are the calculated A_1(LO) and E_1(LO) phonon frequencies with temperatures using ω_0, M_1, and M_2 as fitting parameters (listed in Table 1). The agreement between the theoretical fit and experimental data is quite good. On the one hand, in addition to a blueshift in the Raman frequency of ZnMgO compared with that of ZnO [11,12], we can clearly see the variation of ω_0 with Mg composition, which can be ascribed to the change of the lattice constant. Due to the incorporation of Mg substitutionally on the Zn sublattice, the lattice constant decreases with the increase of Mg composition, resulting in the increase of ω_0. On the other hand, it is noted that the anharmonic constants M_1 and M_2 of A_1(LO) and E_1 (LO) modes in ZnMgO are higher than those in pure ZnO. In ZnMgO, the alloy-induced disorder brings on an increase of phonon density of states (DOS) which leads to the enhancement of the probability of inelastic (anharmonic) scattering between the phonons and substitutional atoms. As a result, the contribution from anharmonicity due to the alloy-induced disorder prevails with increasing Mg composition. Furthermore, the disorder-induced anharmonicity is sensitive to the temperature; the increase of temperature produces a large number of phonons, which also enhances the probability of inelastic (anharmonic) scattering between the phonons and substitutive atoms. Therefore, the alloy-disorder anharmonicity becomes more obvious with the increase of temperature in ZnMgO.

The phonon broadening $\Gamma(T)$ mainly comes from inhomogeneous impurity phonon scattering and anharmonic decay. In analogy to the temperature dependence of Raman shift, the phonon broadening can be described by assuming the decay into two phonons with frequency ω_1 and ω_2 and the symmetric decay into three phonons again [9,10,15]:

$$\Gamma(T) = \Gamma_0 + N_1[1 + n(T,\omega_1) + n(T,\omega_2)] + N_2[1 + 3n(T,\omega_0/3) + 3n^2(T,\omega_0/3)] \quad (3)$$

where Γ_0 denotes a damping contribution due to inherent defect or impurity scattering. The second term displays the asymmetric decay of the three-phonon process, while the third term is the corresponding symmetric decay of the four-phonon process. Anharmonic constants of N_1 and N_2 are the relative probability of the decay into either two or three phonons, respectively. Fig. 3 shows the least-squares fit of Eq. (3) (solid curves) for the temperature-dependent linewidths of the A_1(LO) and E_1(LO) modes in ZnMgO. The fitting parameters Γ_0, N_1, and N_2 have also been given in Table 1. In pure ZnO, Γ_0 of E_1(LO) phonons is found to be larger than that of A_1 (LO) phonons, implying that the E_1(LO) mode is more strongly affected by impurity and/or defect scattering than that of the A_1(LO) mode. However, Γ_0 of A_1(LO) phonons increases much more rapidly with Mg composition than that of E_1 (LO) phonons. As we know, the A_1(LO) mode is polarized along the c axis, whereas the E_1(LO) mode has in-plane polarization [13]. The alloy-induced disorder will have more severe effect on the c axis, resulting in the strong enhancement of the impurity scattering in A_1(LO) phonons of hexagonal ZnMgO.

Fig. 4(a) and (b) display the relative contributions (ratios of M_1/M_2 and N_1/N_2) of the three- and four-phonon processes to

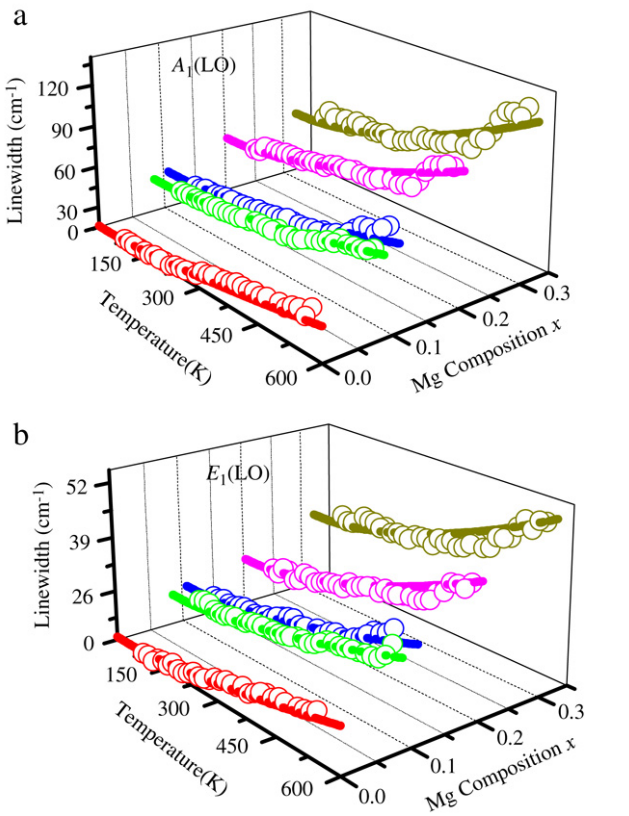

Fig. 3. Temperature-dependent Raman linewidth of the (a) A_1(LO) and (b) E_1(LO) modes in ZnMgO with different Mg compositions. The solid curves are the theoretical calculation results with Eq. (3).

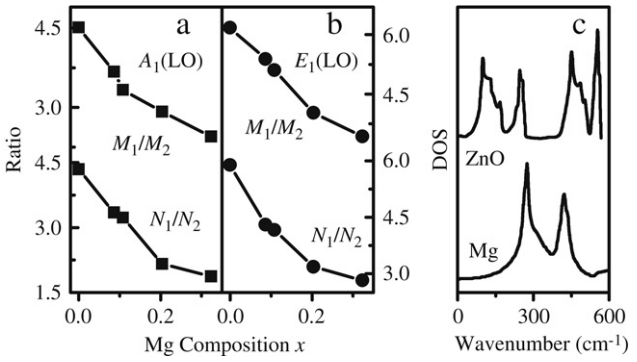

Fig. 4. Mg-composition dependence of ratios M_1/M_2 and N_1/N_2 for the (a) A_1(LO) and (b) E_1(LO) modes in ZnMgO. (c) Calculated phonon DOS of ZnO and Mg atoms.

the total phonon decay for both the A_1(LO) and E_1(LO) modes. It is clear that the ratios are much larger than 1.0, demonstrating that the decay into two phonons is the prevailing process while the four-phonon process makes minor contribution in the anharmonic coupling of the A_1(LO) and E_1(LO) modes. This observation is consistent with the calculated phonon DOS of ZnO [18] shown in Fig. 4(c), where the weak phonon DOS at $\omega_0/3 \sim 200$ cm^{-1} represents less probability of the four-phonon process. However, with increasing Mg composition, the ratios of M_1/M_2 and N_1/N_2 in ZnMgO reduce with the almost same variation. We attribute the change of M_1/M_2 and N_1/N_2 to the fluctuation phonon DOS and the increase of ω_0. The incorporation of Mg in ZnO causes lattice defect and structural disorder, which break down the translational symmetry of ZnO. As a consequence, not only the Brillouin zone-center phonons but also the phonons at Brillouin zone-edges have contributions to the first-order Raman scattering. The increase of the phonon DOS in ZnMgO at ~200 cm^{-1} can be easily observed by the phonon DOS of Mg atoms [19] shown in Fig. 4(c). Furthermore, the increase of ω_0 in ZnMgO causes larger values of ω_1 and ω_2, bringing on the fast reduction of the contribution of the three-phonon process, whereas the blueshift of $\omega_0/3$ leads to an increase in the probability of the four-phonon process. Nevertheless, it should be pointed out that the three-phonon process always dominates the anharmonic shift and broadening of the A_1(LO) and E_1(LO) modes in hexagonal ZnMgO, as expected.

The above observations permit us to have a clear understanding of the temperature effect on the phonon frequency and linewidth in hexagonal ZnMgO, which establishes an experimental base for micro-Raman as a fast, nondestructive, and contactless technique to monitor the local temperature during the operation of ZnMgO-based devices with submicrometer spatial resolution [8,9]. The yielded temperature and Mg-composition-dependent Raman frequency and linewidth can be used to derive calibration curves which return the temperature of the ZnMgO layer as a function of the relative variation of the phonon mode frequency and linewidth with respect to those at room temperature [10]. The local temperature for the ZnMgO-based devices in operation can thus be determined by the calibration curves. Furthermore, the information of the anharmonic effect is also important for the ZnMgO-based light emission device applications, because the degree of lattice disorder in mirrors by Raman microprobe spectroscopy correlates to the strength of facet heating and to the power limit at catastrophic optical mirror damage [8,9].

4. Conclusions

In summary, we have investigated in detail the temperature-dependent micro-Raman scattering of hexagonal $Zn_{1-x}Mg_xO$ ($0 \leq x \leq 0.323$) thin films under the temperature range of 83–578 K grown by PLD on sapphire substrates. The temperature-dependent phonon frequencies and linewidths of the A_1(LO) and E_1(LO) modes in ZnMgO have been obtained through Lorentz fitting. By the aid of a model involving the contributions of the thermal expansion, lattice-mismatch-induced strain, as well as three- and four-phonon coupling, we have clearly illustrated the temperature effect on the phonon frequency and linewidth of hexagonal ZnMgO. It is found that, with increasing Mg composition, the contribution of the four-phonon process increases, while that of the three-phonon process reduces, due to the variation of structural properties and phonon DOS in ZnMgO. The present work demonstrates that the micro-Raman technique is very useful in monitoring the local temperature during the ZnMgO-based device operation with submicrometer spatial resolution.

Acknowledgments

This work was supported by the Natural Science Foundation of China under contract 10734020, the National Minister of Education Program of IRT0524, and the Venture Business Laboratory of Saga University, Japan.

References

[1] A. Tsukazaki, A. Ohtomo, T. Kita, Y. Ohno, M. Kawasaki, Science 315 (2007) 1388.
[2] M.H. Huang, S. Mao, H. Feick, H.Q. Yan, Y.Y. Wu, H. Kind, E. Weber, R. Russo, P.D. Yang, Science 292 (2001) 1897.
[3] T. Nishida, H. Saito, N. Kobayashi, Appl. Phys. Lett. 78 (2001) 3927.
[4] H. Tampo, H. Shibata, K. Maejima, A. Yamada, K. Matsubara, P. Fons, S. Niki, T. Tainaka, Y. Chiba, H. Kanie, Appl. Phys. Lett. 91 (2007) 261907.
[5] B.P. Zhang, N.T. Binh, K. Wakatsuki, C.Y. Liu, Y. Segawa, N. Usami, Appl. Phys. Lett. 86 (2005) 032105.
[6] I. Takeuchi, W. Yang, K.S. Chang, M.A. Aronova, T. Venkatesan, R.D. Vispute, L.A. Bendersky, J. Appl. Phys. 94 (2003) 7336.
[7] J.F. Kong, W.Z. Shen, Y.W. Zhang, C. Yang, X.M. Li, Appl. Phys. Lett. 92 (2008) 191910.
[8] P.W. Epperlein, P. Buchmann, A. Jakubowicz, Appl. Phys. Lett. 62 (1993) 455.
[9] J. Jiménez, E. Martín, A. Torres, J.P. Landesman, Phys. Rev. B 58 (1998) 10463.
[10] A. Link, K. Bitzer, W. Limmer, R. Sauer, C. Kirchner, V. Schwegler, M. Kamp, D.G. Ebling, K.W. Benz, J. Appl. Phys. 86 (1999) 6256.
[11] C. Bundesmann, A. Rahm, M. Lorenz, M. Grundmann, M. Schubert, J. Appl. Phys. 99 (2006) 113504.
[12] J. Huso, J.L. Morrison, H. Hoeck, E. Casey, L. Bergman, T.D. Pounds, M.G. Norton, Appl. Phys. Lett. 91 (2007) 111906.
[13] R. Cuscó, E. Alarcón-Lladó, J. Ibáñez, L. Artús, J. Jiménez, B. Wang, M.J. Callahan, Phys. Rev. B 75 (2007) 165202.
[14] H. Iwanaga, A. Kunishige, S. Takeuchi, J. Mater. Sci. 35 (2000) 2451.
[15] X.D. Pu, J. Chen, W.Z. Shen, H. Ogawa, Q.X. Guo, J. Appl. Phys. 98 (2005) 033527.
[16] Th. Gruber, G.M. Prinz, C. Kirchner, R. Kling, F. Reuss, W. Limmer, A. Waag, J. Appl. Phys. 96 (2004) 289.
[17] G. Carlotti, D. Fioretto, G. Socino, E. Verona, J. Phys.: Condens. Matter 7 (1995) 9147.
[18] J. Serrano, A.H. Romero, F.J. Manjón, R. lauck, M. Cardona, A. Rubio, Phys. Rev. B 69 (2004) 094306.
[19] K. Parlinski, J. Ła zewski, Y. Kawazoe, J. Phys. Chem. Solids 61 (2000) 87.